# Hybrid Modelling of Stimuli-Based and Density-Induced Aggregation in C. elegans

Vellinger, Aymeric; Antonic, Nemanja; Tuci, Elio

*Published in:*
Artificial Life

*DOI:*
10.1162/isal_a_00763

*Publication date:*
2024

*Document Version*
Première version, également connu sous le nom de pré-print

# Hybrid Modelling of Stimuli-Based and Density-Induced Aggregation in *C. elegans*

Aymeric Vellinger[1], Nemanja Antonic[1] and Elio Tuci[1]

[1]University of Namur, Belgium
aymeric.vellinger@unamur.be

## Abstract

In this paper, we study the aggregation of a relatively high number of *C. elegans* roundworms resulting from the interaction between them and a set of external stimuli, namely oxygen and pheromones. Inspired by previous work, we delve into a hybrid modelling approach, simulating the aggregating behaviour of the worms by means of mathematical models, which we solve numerically, and by developing a phenomenological agent-based simulator. Our approaches capture the emergent aggregating behaviour of the worms, resulting in an interesting and coupled interplay between the macroscopic level, where probability distributions measure how the worms aggregate, and the microscopic level, where simple rules guide the agents to form clusters. Overall, our results suggest that there exists a strong correlation between the two approaches, indicating that they are able to capture the same phenomenon, albeit the mathematical model suffering from numerical limitations and the simulator requiring high computational resources. We then leverage our simulator in order to analyse the hypothetical behaviour of worms subject to both stimuli with different response levels, which results in a stronger degree of clustering than the single-stimulus simulation. We believe our framework can help shed light on the complex interactions between very large swarms of *C. elegans*, helping in predicting the emergent properties and reducing the amount of resources needed to run experiments with natural worms.

## Introduction

BABOTS is the acronym of an EU funded project that aims to designing biological animal robots (i.e., BABots) by genetically re-configuring the synaptic connections and neuronal functions of the nematode *C. elegans* (see `https://babots.eu/`). This 1 mm long bacterial-feeding roundworm is a central model organism in biology thanks to its simplicity and genetic tractability (see Ellis et al. (1986); Fire et al. (1998); Chalfie et al. (1994)). It exhibits a simple body plan, comprising 959 somatic cells and 302 neurons arranged in a stereotypical pattern as shown in The C. elegans Sequencing Consortium* (1998); White et al. (1986). The *C. elegans* nervous system is well-characterized and its entire map of synaptic connections, its connectome, provides detailed information about the innate neural circuits that constitute its brain. Editing the connectome by adding new synthetic neuronal connections can alter the function of *C. elegans* neural circuits, modifying whole animal behaviour and even giving rise to novel behaviours. The objective of the BABOTS project is to reprogram the behaviour of the *C. elegans* laboratory strain $N2$ to induce them developing specific collective responses. BABots (i.e., genetically modified worms) will autonomously perform compound tasks designed to meet specific requirements of state-of-the-art vertical farming, such as detecting and attacking invasive pathogens within a contained plant environment. Behavioural and information-based heterogeneity will be exploited to obtain adaptive responses and resilience against harm as illustrated in Firat et al. (2020); Gillet et al. (2019). A methodological framework made of complementary modelling tools will be used to lay the scientific grounds for understanding how individual differences can contribute to the emergence of desired and controllable collective responses.

Generally speaking, the high genetic diversity within *C. elegans* makes it an excellent model organism for investigating social behaviours and their impact on swarming. For instance, genetic factors can regulate chemotaxis, the process by which nematodes navigate chemical gradients in their environment Iino and Yoshida (2009), and also play a role in oxygen sensing mechanisms, governing how nematodes respond to changes in oxygen levels Gray et al. (2004). Modifications in the genome can also enhance aggregation behaviour, as shown in Wan et al. (2019). Multiple studies have modelled aggregation processes in *C. elegans* using systems of ordinary differential equations Chen and Ferrell (2021) and partial differential equations, particularly employing the Keller-Segel model Keller and Segel (1970); Demir et al. (2020); Liebchen and Löwen (2018); Wang (2010); Avery et al. (2021). These equations are continuous and differentiable, hence smooth, while the actual distribution of worms is by nature discontinuous and lumpy. This discrepancy between model assumptions and physical-

world observations prompts the exploration of alternative modelling approaches that can better capture the complexities of worm behaviour.

The objective of this paper is to describe the tools that we have recently developed to model and to analyse group responses in biological systems by operationally defining the mechanisms underpinning the individual behaviours. In particular, we illustrate the characteristics of a macroscopic (mathematical) and a microscopic (an agent-based) model and we evaluate them with respect to how effectively they reproduce aggregation dynamics in populations on *C. elegans*. At the microscopic level, simulations model the behaviour of individual agents, representing *C. elegans*, allowing for a detailed examination of their actions and interactions Iino and Yoshida (2009); Ding et al. (2020); Matsuoka et al. (2008); Palyanov et al. (2018). Meanwhile, at the macroscopic scale, mathematical models provide a holistic view by treating the entire population as a single entity, capturing emergent properties and collective behaviours Szigeti et al. (2014); Coburn et al. (2013); Sugi et al. (2019). An important aspect of our analysis is dedicated to a quantitative evaluation of the similarities between the population dynamics observed in the two types of model. Reliable modelling tools are crucial in order to gain better understanding of the underlying principles governing systems that are influenced by complex interactions with a large number of individuals. By using complementary modelling techniques, we investigate how the collective outcome is affected by multiple elements, including different engineered mobility patterns and sensori-motor responses and also by the characteristics of the physical and social environment.

The group dynamics that we target in this study are those related to aggregation triggered by two main factors: the level of ambient oxygen $[O_2]$ and the level of pheromones, impacting the direction of the worms. The former has been well established as a pivotal environmental parameter governing the aggregation of the $npr-1$ and $N2$ worms Demir et al. (2020); the latter is assumed to be produced by $L1$ worms, and causes the aggregation through an attractant and a repellent pheromone secreted by the nematode Avery et al. (2021). We take inspiration from two mathematical models for the two types of aggregation in the literature in order to build an agent-based phenomenological simulator, which displays qualitatively and quantitatively similar trends to those of the mathematical models, while matching the experiments with natural worms. This tool offers great flexibility and allows to reliably replicate complex interactions in the presence of a high density of *C. elegans*. In addition to the description of the two models, a further original scientific contribution of this paper is the illustration of a set of experiments, run with the micro model, that quantitatively describe the type of aggregation dynamics observed when both the level of oxygen and of the attractant and repellent pheromones influence the pattern of movements of simulated worms.

## Worms movement

Two distinct mathematical models, based on partial differential equations (**PDEs**), have been proposed by different researchers to model the evolution of worm density over time. These equations describe by inference the movement of the worms, since changes in the density maintain the total amount of worms constant.

Demir et al. (2020) describe the evolution of worms density through time proportionally to the divergence of a vector field described by the oxygen concentration $O$, their velocity $V$ and the worm density $W$:

$$\frac{dW}{dt} = \frac{1}{2\tau}\nabla \cdot [V\nabla OW] \tag{1}$$

On the other hand, Avery et al. (2021) describe the evolution of worm density over time using a Fokker-Planck equation. This equation depicts how the probability density of worms in a 2D space is affected by external factors, in this case, the concentration of pheromones, acting as a potential $V$:

$$\frac{dW}{dt} = \nabla \cdot [W\nabla V + \sigma\nabla W] \tag{2}$$

In order to translate the differential equations into an agent-based model, we implement the movement of the nematodes according to a continuous time persistent random walk without external directional bias Patlak (1953). The position $\mathbf{p}_t$ and the direction $\mathbf{d}_t$ at time $t$ are computed in the following:

$$\mathbf{p}_t = \mathbf{p}_{t-1} + \mathbf{d}_t \cdot v; \tag{3}$$

$$\mathbf{d}_t = \lambda \cdot \mathbf{d}_{t-1} + (1-\lambda) \cdot \mathbf{u}_t; \tag{4}$$

$$\mathbf{u}_t = (\cos(\alpha), \sin(\alpha)); \tag{5}$$

where $v$ being the step size, $\lambda = 0.8$ is the persistence factor, and $\alpha$ is sampled from a uniform distribution over the interval $[0, 2\pi]$. One advantage of using this random walk to describe the movement of *C. elegans* is that it naturally incorporates the pirouette rate, an important feature of nematodes walks, as shown in Pierce-Shimomura et al. (1999). This is obtained with the persistence factor $\lambda$, with the probability for an agent to perform a pirouette being inversely proportional to $\lambda$.

In Figure 1, we show the distribution of the trajectory taken by a sample of four agents after 2000 steps. Agents 1, 3 and 4 display a preference for a direction and, given the importance of pirouettes in the movement of the animals, they tend to follow a single direction and its opposite. On the contrary, agent 2 displays a more uniform distribution, showing lower directional preferences compared to the other agents. These directional distributions fairly replicate those of the worms observed in laboratory conditions by Peliti et al. (2013). The general overview of this simplistic random walk allows us to say that it confidently replicates

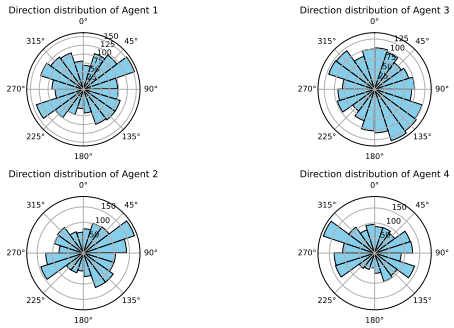


Figure 1: Sample of agents directions distribution ran over 2000 steps for $\lambda = 0.8$. Histograms display the trajectories shown by single agent. Counts within a bin are obtained by summing step-by-step heading direction of the agent within an interval specified by the bins.

the behaviour of a $N2$ laboratory *C. elegans* without the necessity to introduce other environmental factors (e.g., food, pheromones).

In order to model the effects of environmental factors that generate attraction or repulsion responses, we integrate into the simulator terms that bias the computation of the agent direction $\mathbf{d}_t$ toward or away from these factors. In particular, the direction $\mathbf{d}_t$ is computed by attraction forces toward the highest concentration of attractant $A_t$ and repulsion forces away from the highest concentration of repellent $R_t$, whenever the environmental factors causing them are within the agent's sensing range $s$.

When an agent is affected by attraction forces its direction $\mathbf{d}_t$ is computed as follows:

$$\mathbf{d}_t = \lambda \cdot \mathbf{d}_{t-1} + (1-\lambda) \cdot (\mathbf{u}_t + \mu A_t \cdot \mathbf{b}_A); \tag{6}$$

where $\mathbf{b}_A$ represents the bias vector towards the attractant at time $t$; $A_t$ being the highest quantity of attractant at time $t$ in a sensing range $s$, $\mu \geq 0$ the drift factor representing the strength of attraction.

When an agent is affected by repulsion forces its direction $\mathbf{d}_t$ is computed as follows:

$$\mathbf{d}_t = \lambda \cdot \mathbf{d}_{t-1} + (1-\lambda) \cdot (\mathbf{u}_t + \mu R_t \cdot \mathbf{b}_R); \tag{7}$$

$R_t$ being the highest quantity of repellent at time $t$ in a sensing range $s$ and $\mathbf{b}_R$ representing the bias vector away from the repellent. $\mathbf{b}_A$ and $\mathbf{b}_R$ are computed as follows:

$$\mathbf{b}_A = (\cos(\theta), \sin(\theta)); \tag{8}$$

$$\mathbf{b}_R = (\cos(\theta + \pi), \sin(\theta + \pi)); \tag{9}$$

with:

$$\theta = \arctan\left(\frac{\mathbf{w}_t^y - \mathbf{p}_t^y}{\mathbf{w}_t^x - \mathbf{p}_t^x}\right); \tag{10}$$

where $\mathbf{w} \in \{\mathbf{A}, \mathbf{R}\}$ are the coordinates of the highest concentration of stimulus within a sensing range $s$ at time $t$ and $\mathbf{p}$ the coordinate of the agent at time $t$.

## Aggregation responses

Aggregation in different strains of *C. elegans* is promoted by external interaction within their environment. In order to model these interactions, a differential equation is introduced to model the change in the concentration of external stimuli, therefore transforming the set of equations in a Keller-Segel model. A Keller-Segel model Keller and Segel (1970) is a system of coupled partial differential equations, where one set of equations describes the diffusion of some chemical substances, and another set describes the movement of organisms in response to these chemical gradients. In the following, we present two Keller-Segel systems from the literature and introduce their agent-based equivalents in the microscopic model.

### Oxygen-induced aggregation

Authors in Demir et al. (2020) show that the velocity of a $npr-1$ worm depends on the sensed local oxygen level and provide a simplified parabolic expression of velocity $V(O)$, where $O$ is the local level of oxygen. They find this relationship through experiments in the presence of a relatively high number of worms and sensors capable of detecting the oxygen level in an agar plate. Their results indicate that if a given instability criterion, entirely dependant on the initial density of worms and ambient oxygen levels, is satisfied, then aggregation occurs as the result of the instability of the system. In particular, the PDE relative to $O$ is as follows:

$$\frac{dO}{dt} = D_O \nabla^2 O - k_c W + f(O_{am} - O) \tag{11}$$

We solve the system composed of Equations 1 and 11 by implementing the finite difference method in a grid, where each spacial coordinate of length $l = 1cm$ is divided in $n = 512$ intervals, with $dt = 0.01$ and $t \in [0, 500000]$. Similarly to what authors in Demir et al. (2020) do, we implement periodic boundary conditions in both axis. To implement the flux evolution of the oxygen in the agent-based simulator, we discretise the environment in a $n = 128$ grid to model the spatial dynamics within the system and to facilitate the application of mathematical methods (such as solving partial differential equations), in a computationally efficient manner. This technique has already been used in an efficient way for biological representation in Cruz and Kemp (2021); Marzban et al. (2021). By discretising the environment, we transform the continuous spatial domain into a discrete representation, enabling us to implement numerical algorithms for solving differential equations. Hence, we numerically solve the aforementioned system within each grid cell at each time step to simulate the dynamic oxygen variation of the system, allowing us to solve the PDE in real time.

Formally, we approximate the Laplacian operator using a centered finite difference method as:

$$\nabla^2 O^{i,j} \approx \frac{O^{i+1,j} + O^{i-1,j} - 4O^{i,j} + O^{i,j+1} + O^{i,j-1}}{h^2} \tag{12}$$

with $h = \frac{l^2}{n^2}$. Each point $(i, j)$ in the oxygen grid $O \in \mathbf{R}^{n \times n}$ is then updated as follows:

$$O_t^{i,j} = O_{t-1}^{i,j} + f(O_{am} - O_{t-1}^{i,j}) - W_{t-1}^{i,j} k_c + D_O \nabla^2 O_{t-1}^{i,j} \tag{13}$$

We implement the continuous persistent random walk without external bias, as worms are not directly attracted or repelled by the presence of oxygen, with a step size of

$$V = aO^2 + bO + c \tag{14}$$

where $a = 1.89, b = -0.398$ and $c = 2.25E - 2[cm/s]$ have been estimated as to approximate the velocity profile of the worms with respect to the local oxygen level Demir et al. (2020).

### Pheromone-based aggregation

Avery et al. (2021) models the aggregation of a population of $L1$ worms guided by the secretion of repellent and attractant pheromones. In particular, $L1$ worms produce a short-range attractant and a longer range repellent, though both degrade over time due to evaporation and diffusion. The authors find that it is sufficient to account for the evolution through time of the local density of worms $W$, repellent $U_r$ and attractant $U_a$, hence they develop a Keller-Segel model. In particular, they model the evolution of pheromone $p \in \{r, a\}$ as the sum of three terms: the decrease due to the evaporation, the diffusion and the secretion of pheromones.

$$\frac{dU_p}{dt} = -\gamma_p U_p + D_p \nabla^2 U_p + s_p W \tag{15}$$

Moreover, Equation 2 describes the evolution of worm density through the divergence of two terms which account for: i) the interaction between the worms and the potential $V$, and ii) the change in worm density guided by the random movement of the worms. In particular, the potential $V$ is composed itself of two potentials:

$$V = V_U + V_W \tag{16}$$

where the two terms are, intuitively, the potential created by the diffusion of the pheromones and the worms trying to squeeze together as tightly as possible. We solve the system of Equations 2 and 15 following the same methodology described in the previous section, but extending the time interval to $t \in [0, 500000]$ as to cope with the slower aggregation process observed when compared to the study conducted by Demir et al. (2020).

We develop the agent-based model by overlaying on the environment two grids with $n = 128$ intervals per each spacial coordinate. Let $A, R \in \mathbf{R}^{n \times n}$ being the matrices representing the attractant and repellent grid, respectively. Then, we proceed with the update of the grids leveraging the approximation of the Laplacian operator as described in Equation 12:

$$A_t^{i,j} = A_{t-1}^{i,j} + s_a W_{t-1}^{i,j} - \gamma_a A_{t-1}^{i,j} + D_A \nabla^2 A_{t-1}^{i,j} \tag{17}$$

$$R_t^{i,j} = R_{t-1}^{i,j} + s_r W_{t-1}^{i,j} - \gamma_r R_{t-1}^{i,j} + D_R \nabla^2 R_{t-1}^{i,j} \tag{18}$$

### Multi-stimulus scenario

To make an agent react to both oxygen and pheromone, we change the velocity $V$ by combining and weighting it with the parameter $h \in [0, 1]$ as follows:

$$V = (1 - h) \cdot V_\phi + h \cdot (V_O \cdot 10^{-2}) \tag{19}$$

where $V_\phi = V_a + V_r$ and $V_O$ is multiplied by a factor to account for the numerical difference between the two terms. Our approach implies that it is numerically possible to relate the reaction of the worms to oxygen and to pheromones. In particular, this multi-stimulus simulation aims to more accurately replicate the behaviour of natural worms, which are capable of sensing both oxygen and pheromones like $npr - 1$, thereby allowing for the evaluation and discovery of the significance of each interaction in aggregation.

## Metrics

In order to quantify the degree and type of aggregation across the different types of stimuli, we borrow and adapt from the literature the clustering metric Gauci et al. (2014), by defining it as the proportion of worms that belong to a cluster (originally, the size of the largest cluster) and the total amount of worms. This metric is adapted in such a way to account for multiple clusters, which emerge when the aggregation process gives rise to patterns such as dots. In our agent-based simulator, this metric is calculated by examining clusters of size at least $4$, as we consider this to be the minimum number of agents necessary for a cluster to be formed, while in the results of the mathematical models we consider clusters of at least 2 neighbouring cells with a density above the average density across the grid.

Furthermore, we analyse the distribution of the worms, in particular looking at the kurtosis of the distribution, which tells us how far from a Gaussian the distribution is. By combining the clustering metric and the kurtosis, we are able to understand the nature of our aggregation. A high kurtosis indicates that the distribution is Gaussian, therefore the aggregation is weak. A relatively low kurtosis, on the other hand, combined with a high clustering metric, implies that the aggregation is stronger.

## Results

In this section, we show the results of aggregation dynamics driven by either the level of oxygen or of a combination of attractant and repellent pheromones, by focusing on the correspondence between the results generated with the macro

Table 1: Parameters used to run the simulations with the micro model.

| Parameters | values |
|---|---|
| initial density $W_0$ | $[40, 190]$worm/mm$^2$ |
| random walk persistence $\lambda$ | $0.8$ |
| maximum worms per cell $w_{\text{max}}$ | $4$ |
| random worm movement $\sigma$ | $0.0005555[\text{mm}^2\text{s}^{-1}]$ |
| **oxygen** | |
| diffusion constant $D_O$ | $0.002[\text{mm}^2\text{s}^{-1}]$ |
| consumption $k_c$ | $0.00073[\text{mm}^2\text{s}^{-1}]$ |
| ambient level $O_{am}$ | $0.21$ |
| penetration rate $f$ | $0.65[\text{s}^{-1}]$ |
| **attractant** | |
| decay rate $\gamma_a$ | $0.01[\text{s}^{-1}]$ |
| diffusion constant $D_a$ | $0.0001[\text{mm}^2\text{s}^{-1}]$ |
| concentration scale $\alpha_a$ | $15[\text{mm}^{-2}]$ |
| strength $\beta_a$ | $0.00111[\text{mm}^2\text{s}^{-1}]$ |
| secretion rate $s_a$ | $0.0001[\text{mm}^{-2}\text{s}^{-1}]$ |
| **repellent** | |
| decay rate $\gamma_r$ | $0.001[\text{s}^{-1}]$ |
| diffusion constant $D_r$ | $0.001[\text{mm}^2\text{s}^{-1}]$ |
| concentration scale $\alpha_r$ | $15[\text{mm}^{-2}]$ |
| strength $\beta_r$ | $-0.001111[\text{mm}^2\text{s}^{-1}]$ |
| secretion rate $s_r$ | $0.00001[\text{mm}^{-2}\text{s}^{-1}]$ |

(i.e., the mathematical) and the micro (i.e., the agent-based simulation) model. The comparative analysis of the aggregation dynamics triggered by the level of oxygen is based on the observation and description of the final worm density distributions for different initial conditions. The comparative analysis for the aggregation dynamics triggered by the level of pheromones is based on the description of the evolution through time of the worm density and of the external stimuli (i.e., oxygen and pheromone). The changes in time of both worm density and external stimuli are diffusion processes that give rise to the emergence of Turing patterns Turing (1990). This phenomenon occurs when two chemicals, typically referred to as "activator" and "inhibitor", interact within a system undergoing diffusion. We also illustrate the aggregation dynamics observed with the micro model in a multi-stimulus scenario in which the interactions between simulated *C. elegans* are determined by both the level of oxygen and of attractant and repellent pheromones. The parameters of the micro model used to run the simulations illustrated in this section are shown in Table 1.

## Aggregation dynamics triggered by oxygen concentration

To evaluate how closely our results match those illustrated in Demir et al. (2020), and how closely the macro (mathematical) model aligns with the micro (agent-based) model regarding the *C. elegans* reaction to oxygen, we analyse the final worm density distribution ($W_T$) in different conditions that differ for the initial worm density ($W_0$) measured in number of worms per $mm^2$ (i.e., worm/mm$^2$). In particular, in the micro model we look at conditions with initial worm densities $W_0 \in [40, 190]$worm/mm$^2$ at intervals of $5$worm/mm$^2$. For each different density, we run $10$ differently seeded independent replications of the experiment and we average the results. In the macro model, we look at the conditions with initial worm densities $W_0 \in [40, 85]$worm/mm$^2$ at intervals of $5$worm/mm$^2$. The difference in the range of initial densities between the macro and the micro model is due to the macro model being limited by the instability criterion, which restricts the aggregation phenomenon to a range of initial densities smaller than the range of the simulator.

In Figure 2, we show the oxygen-induced aggregation patterns (scatter plots) and the final worm density $W_T$ distribution (histograms) for the micro model (orange graphs, with $T = 1,500$ time steps) and the macro model (blue graphs, $T = 50,000$ time steps) in different conditions. In particular, in Figure 2a, 2b, and 2c, referring to the micro model, the initial worm density $W_0$ is set to $W_0 = 40$ worm/mm$^2$, $W_0 = 130$ worm/mm$^2$, and $W_0 = 190$ worm/mm$^2$, respectively. In Figure 2d, 2e, and 2f, referring to the macro model, the initial worm density $W_0$ is set to $W_0 = 40$ worm/mm$^2$, $W_0 = 65$ worm/mm$^2$, and $W_0 = 80$ worm/mm$^2$, respectively. First, we see that we have successfully replicated the experiments conducted by Demir et al. (2020). Equivalences with authors previous work can be seen in Figure 2d, 2e and 2f that display similar patterns than in Figure 2d (p.5) and Figure 3c (p.8) of Demir et al. (2020). As far as it concerns the similarities between the models, the graphs show that there are strong similarities between the final worm density distributions ($W_T$) and Turing patterns observed in the two models for progressively higher values of $W_0$. We can also observe that for low initial density (see Figure 2a and 2d), the histograms describe a positively skewed bimodal distribution. This indicates that a lot of empty or low density cells can be found in between clusters of worms. For high initial densities (see Figure 2c and 2f), we observe a negatively skewed distribution. This indicates that the aggregation dynamics tend to result in a fully connected cluster with empty spaces in between. Finally, we observe that the evolution of the worm density distribution passes through a balanced bimodal distribution representing a turning point between the hole and dotted Turing patterns (see Figure 2b and 2e).

To further investigate how similar the aggregation dynamics are between the micro and macro model, we compute the kurtosis and the clustering metric for different conditions defined by the worm initial density $W_0$. The results shown in Figure 3, indicate that as far as it concerns the kurtosis (see Figure 3a) the two models are characterised by the same parabolic trend, even if the curve of the micro model

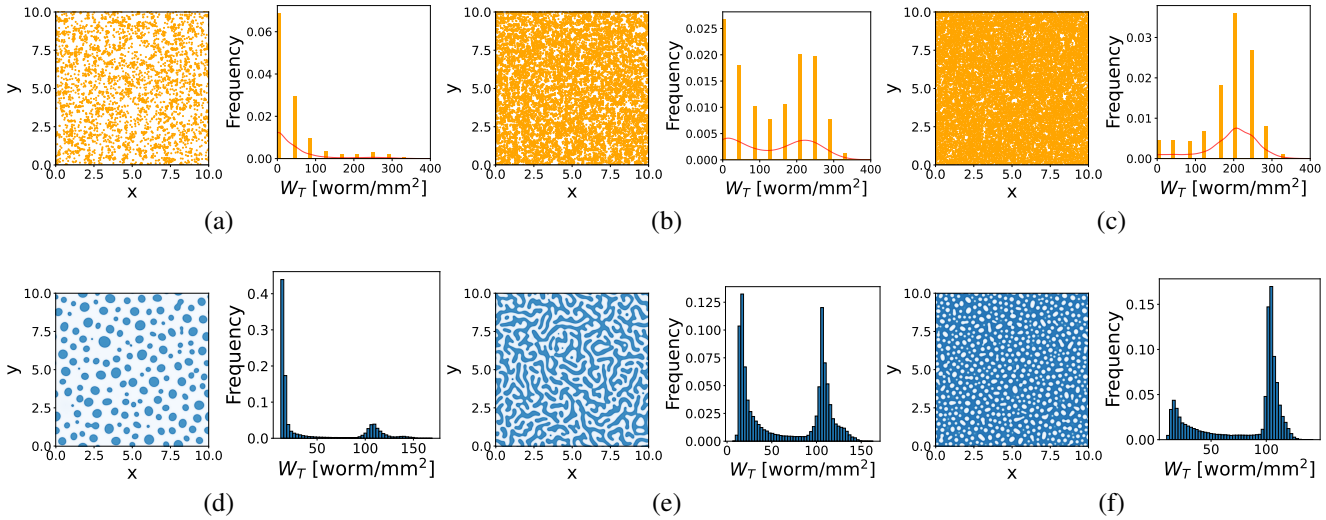


Figure 2: Graphs showing the oxygen-induced aggregation patterns (scatter plots) and final worm density $W_T$ distribution (histograms) for the micro model (orange graphs) and the macro model (blue graphs) for the following different initial density conditions: a) $W_0 = 40$; b) $W_0 = 130$; c) $W_0 = 190$; d) $W_0 = 40$; e) $W_0 = 65$; f) $W_0 = 80$ [worm/mm$^2$]. Graphs about the final worm density distribution report the average values over 10 differently seeded runs. The environment size visualised in the scatter plots is 10 mm $\times$ 10 mm.

covers a broader set of conditions and it is translated on the x-axis with respect to the macro model. With regard to the clustering metric (see Figure 3b), the two models are characterised by the same increasing trend for progressively larger values of $W_0$. The combined information from kurtosis and clustering confirms that for low values of $W_0$ the final worm density distribution is characterised by low density or empty cells between cells occupied by clusters of worms. On the other hand, for high values of $W_0$, the final worm density distribution is characterised by a large number of cells occupied by fewer clusters of worms, up to the emergence of a single cluster for the highest considered value of $W_0$ (see also Figure 2c, and 2f). In order to assess the correlation between the final density distributions observed in the two models, we compute the squared histogram intersection ($r$) of these distributions, by computing the squared differences of their corresponding bin values and by adding them together. This metric $r$ is thus computed as follows:

$$r = \sum_{i=1|A[i]\neq 0 \wedge B[i]\neq 0}^{n} \left( (A[i] - B[i])^2 \right) \qquad (20)$$

where $A, B \in \mathbf{R}^n$ are the values of the histograms and $n$ is the number of bins. The results shown in Figure 3c tell us that there is a strong correlation of the final worm density distributions for low values of $W_0$, and weaker correlations for high values of $W_0$. That can be explained by the physical limitations in the micro model which makes it impossible for the agents to penetrate one into each other, and by the size of the grid used to conduct the simulations, which is coarser in the micro model than in the macro model.

## Aggregation dynamics triggered by pheromones concentration

In this section, we describe the aggregation dynamics observed in both models by worms attracted by pheromones generated forces. First, the mathematical model detailed in Avery et al. (2021) has been successfully replicated. This can be seen by looking at Figure 4c, which shows the final worm distribution (Turing patters) for the macro model. The patterns shown in Figure 4c are similar to those shown in Figure 3D (p.11) and Figure 5 (p.13) of Avery et al. (2021). As far as it concerns the similarities between the models, it is important to highlight that the main difference between oxygen based and pheromone based aggregation is that the latter tends to form round and unconnected clusters, hence a dotted Turing pattern, while the former allows the formation of different patterns, as previously discussed. Thus, instead of conducting an analysis based on the initial density, we look for the evolution through time of the clustering metric illustrated above.

In particular, we analyse the correlation between the micro and macro model by plotting the evolution of the clustering metric over time with an initial density $W_0 = 80$ worm/mm$^2$ in Figure 4. The clustering metric of the mathematical model exhibits a hyperbolic tangent, which can be ideally divided in three phases: a first plateau due to noise present at initialisation; a relatively quick growth due to the aggregation process; a second plateau due to the maximum aggregation being reached. Conversely, the simulator portrays an evolution characterised by only the last two phases and by a slower growth, which is closer to the

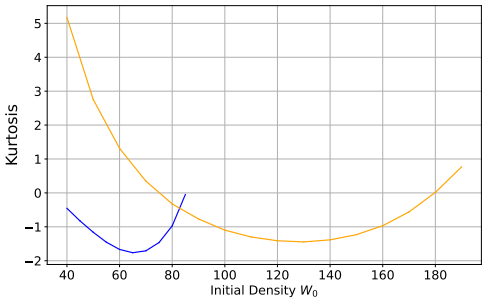


(a)

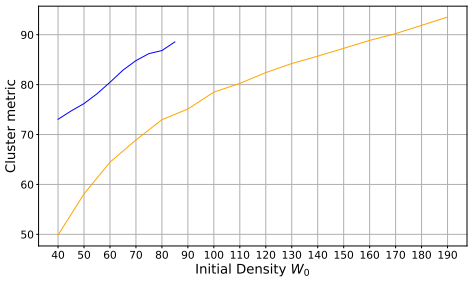


(b)

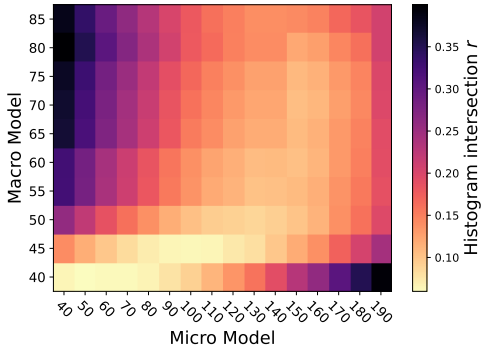


(c)

Figure 3: Graphs showing: a) kurtosis of the final worm density distribution $W_T$ for different conditions defined by the initial density $W_0$ for the macro model (blue line) and micro model (orange line); b) clustering metric of the final worm density distribution for different conditions defined by the initial density for the macro model (blue line) and micro model (orange line); c) Heatmap of the squared histogram intersection of the final worm density $W_T$ distribution in the micro model ($x$ axis) and the macro model ($y$ axis) for oxygen induced aggregation dynamics. Lower values (in yellow) correspond to a stronger correlation between the histograms, while values superior to $0.25$ (in black) imply little to no correlation.

behaviour of natural *C. elegans*. This difference can be best explained by the spatial properties of our agent-based simulator, which allows the agents to reconfigure their position directly based on the nearest source of sensed pheromones. Moreover, the slower growth is directly associated to spatial-

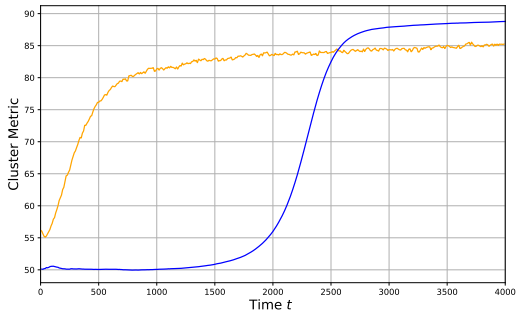


(a)

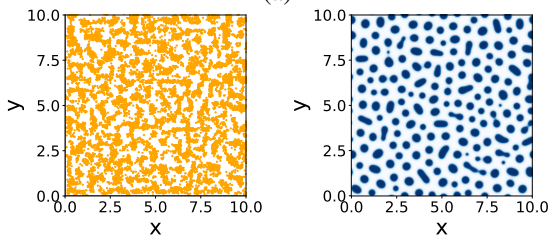


(b) (c)

Figure 4: Graphs for the pheromone-based aggregation showing: a) the evolution (from 0 s to 4,000 s) of the clustering metric for $W_0 = 80$worm/mm$^2$ in both the micro (orange line) and macro model (blue line); b) and c) the final worm distribution (Turing patters) for the micro (orange scatter plot) and the macro (blue scatter plot) model.

ity, since the agents need to physically move in the desired direction, while bounded by the same speed as the agents in the mathematical model. Despite this difference, both models show a similar clustering metric within the same range at initial and final time steps.

## Multi-stimulus scenario

We investigate the influence of the parameter $h$ from Equation 19 in the multi-stimulus scenario, examining the impact of different values of $h$ ranging from $h = 0$ (solely pheromones) to $h = 1$ (solely oxygen) on the worms aggregation dynamics across different values of $W_0$. We show the heatmap of the clustering metric across values of $h \in [0, 1]$ and of initial density $W_0 \in [40, 190]$worm/mm$^2$ in Figure 5a, where red dots indicate the maximum value of the clustering metric for each value of $W_0$. In particular, the maxima are achieved for values of $h \in [0.4, 0.7]$, thus indicating that the presence of both stimuli consistently promotes aggregation by maximising the clustering metric. Moreover, Figure 5b shows the kurtosis in the multi-stimulus scenario across values of $h \in [0, 1]$ and of initial density $W_0 \in [40, 190]$worm/mm$^2$, where red dots indicate the minimum values of kurtosis. In particular, values of $h \in [0.2, 0.9]$ minimise kurtosis across the values of $W_0$, indicating that the multi-stimulus scenario yields larger clusters compared to those formed under the exclusive influ-

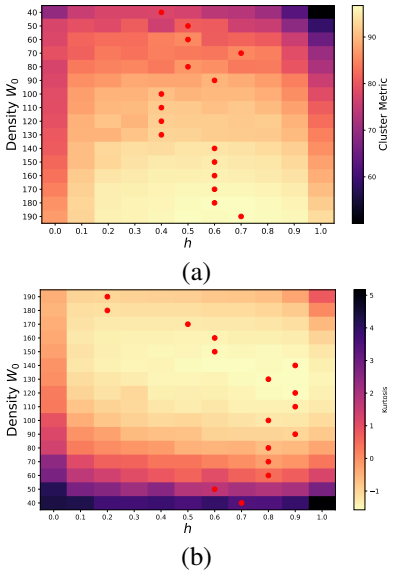


Figure 5: Heatmaps showing: a) the clustering metric and b) the kurtosis, for different values of $W_0 \in [40, 190]$worm/mm$^2$ (y-axis) and $h \in [0, 1]$ (x-axis) in the multi-stimulus scenario. Red dots indicate the maximum clustering metric (a) and the minimum kurtosis (b) for each value of $W_0$ across the values of $h$.

ence of oxygen or pheromones. Such wider clusters denote a higher degree of aggregation, suggesting a robust synergy between multiple stimuli sensation in driving cohesive behaviour among the agents.

## Conclusion and Future work

In this study, we investigated the correspondence between agent-based simulation (microscopic model) and mathematical modelling (macroscopic model) to better understand the aggregation behaviour of *Caenorhabditis elegans* (*C. elegans*) under different environmental stimuli (i.e., level of oxygen and of attractant and repellent pheromones).

For oxygen-induced aggregation, we adapted the mathematical model illustrated in Demir et al. (2020) describing the evolution of worm density in response to local oxygen levels. We implemented this model in a simulation framework using FLAMEGPU 2 Richmond et al. (2024) and compared the resulting density distributions with those obtained from the macro model. Our analysis reveals a strong correlation between the two approaches, particularly at low initial densities. However, discrepancies in the breadth of the distribution suggest potential limitations in the macro model's ability to capture the full complexity of the biological system. We argue this difference is due to the simplicity of the model with respect to the natural *C. elegans*.

Similarly, for pheromone-based aggregation, we leveraged a Keller-Segel model to simulate the dynamics of attractant and repellent pheromones secreted by the worms as in Avery et al. (2021). By comparing the evolution of the percentage of worms aggregated over time, we found consistent trends between the macro and the micro model. However, we also observed slight variations in the rate of aggregation. These discrepancies may arise from simplifications or assumptions inherent to the mathematical model.

Overall, the strong correlation between the micro and macro models suggests that the two approaches are complementary: the latter aids in the study of the aggregation from a probabilistic point of view; the former, on the other hands, enhances the understanding of aggregation from a set of simple rules that each agents follows.

Additionally, our multi-stimulus simulation framework allows us to investigate the impact of environmental stimuli on aggregation behaviour. By adjusting the response level of worms to the stimuli, we find that the multi-stimulus simulation is able to outperform the simulation leveraging a single stimulus in terms of the percentage of aggregated worms and the size of the clusters. This implies that the inclusion of different stimuli may aid in strengthening the aggregation response of *C. elegans* and allows us to predict the collective behaviour of the animals while modulating the concentration of stimuli. We believe our work can provide useful insights to the BABOTS project, since it allows to predict the emergent behaviours of relatively large amounts of *C. elegans* helping in reducing the number of experiments with natural worms, thus saving time and resources.

In future work, we plan on modelling heterogeneous swarms of worms, where group heterogeneity is implemented via sub-populations of worms whose sensitivity to a specific stimulus is pronounced. We argue that the use of such stimuli can play an important role in the development of swarms where a relatively small percentage of modified worms are able to act as an informed minority, guiding the uninformed majority of worms towards a designated goal. Moreover, limited experiments with natural *C. elegans* to verify the results obtained from such an analysis may help us in achieving fully controllable swarms of *C. elegans*.

## Material

`https://github.com/BABots-Project/worm-numerical-analysis`
`https://github.com/BABots-Project/FLAMEGPU2-BABots`

## Acknowledgements

The BABots project has received funding from the Horizon Europe, PathFinder European Innovation Council Work Programme under grant agreement No 101098722. Views and opinions expressed are however those of the authors only and do not necessarily reflect those of the European Union or European Innovation Council and SMEs Executive Agency (EISMEA). Neither the European Union nor the granting authority can be held responsible for them.

# References


Avery, L., Ingalls, B., Dumur, C., and Artyukhin, A. (2021). A keller-segel model for c elegans l1 aggregation. *PLOS Computational Biology*, 17(7):1–25.

Chalfie, M., Tu, Y., Euskirchen, G., Ward, W. W., and Prasher, D. C. (1994). Green fluorescent protein as a marker for gene expression. *Science*, 263(5148):802–805.

Chen, Y. and Ferrell, J. E. (2021). *C. elegans* colony formation as a condensation phenomenon. *Nature Communications*, 12(1):4947.

Coburn, L., Cerone, L., Torney, C., Couzin, I. D., and Neufeld, Z. (2013). Tactile interactions lead to coherent motion and enhanced chemotaxis of migrating cells. *Phys Biol*, 10(4):046002.

Cruz, D. A. and Kemp, M. L. (2021). Hybrid computational modeling methods for systems biology. *Progress in Biomedical Engineering*, 4(1):012002.

Demir, E., Yaman, Y. I., Basaran, M., and Kocabas, A. (2020). Dynamics of pattern formation and emergence of swarming in caenorhabditis elegans. *Elife*, 9:e52781.

Ding, S. S., Muhle, L. S., Brown, A. E., Schumacher, L. J., and Endres, R. G. (2020). Comparison of solitary and collective foraging strategies of caenorhabditis elegans in patchy food distributions. *Philosophical Transactions of the Royal Society B*, 375(1807):20190382.

Ellis, H. M., Horvitz, H. R., et al. (1986). Genetic control of programmed cell death in the nematode *c. elegans*. *Cell*, 44(6):817–829.

Firat, Z., Ferrante, E., Gillet, Y., and Tuci, E. (2020). On self-organised aggregation dynamics in swarms of robots with informed robots. *Neural Comp. & App.*

Fire, A., Xu, S., Montgomery, M. K., Kostas, S. A., Driver, S. E., and Mello, C. C. (1998). Potent and specific genetic interference by double-stranded rna in caenorhabditis elegans. *nature*, 391(6669):806–811.

Gauci, M., Chen, J., Li, W., Dodd, T. J., and Groß, R. (2014). Self-organized aggregation without computation. *The International Journal of Robotics Research*, 33(8):1145–1161.

Gillet, Y., Ferrante, E., Firat, Z., and Tuci, E. (2019). Guiding aggregation dynamics in a swarm of agents via informed individuals: an analytical study. In et al., J. B., editor, *Int. Conf. on Artificial Life (ALife)*. MIT Press. 590–597.

Gray, J. M., Karow, D. S., Lu, H., Chang, A. J., Chang, J. S., Ellis, R. E., Marletta, M. A., and Bargmann, C. I. (2004). Oxygen sensation and social feeding mediated by a *c. elegans* guanylate cyclase homologue. *Nature*, 430(6997):317–322.

Iino, Y. and Yoshida, K. (2009). Parallel use of two behavioral mechanisms for chemotaxis in caenorhabditis elegans. *Journal of Neuroscience*, 29(17):5370–5380.

Keller, E. F. and Segel, L. A. (1970). Initiation of slime mold aggregation viewed as an instability. *J Theor Biol*, 26(3):399–415.

Liebchen, B. and Löwen, H. (2018). Synthetic chemotaxis and collective behavior in active matter. *Accounts of Chemical Research*, 51(12):2982–2990.

Marzban, S., Han, R., Juhász, N., and Röst, G. (2021). A hybrid pde–abm model for viral dynamics with application to sars-cov-2 and influenza. *Royal Society open science*, 8(11):210787.

Matsuoka, T., Gomi, S., and Shingai, R. (2008). Simulation of *c. elegans* thermotactic behavior in a linear thermal gradient using a simple phenomenological motility model. *Journal of theoretical biology*, 250(2):230–243.

Palyanov, A., Khayrulin, S., and Larson, S. D. (2018). Three-dimensional simulation of the caenorhabditis elegans body and muscle cells in liquid and gel environments for behavioural analysis. *Philosophical Transactions of the Royal Society B: Biological Sciences*, 373(1758):20170376.

Patlak, C. S. (1953). Random walk with persistence and external bias. *The bulletin of mathematical biophysics*, 15:311–338.

Peliti, M., Chuang, J. S., and Shaham, S. (2013). Directional locomotion of *c. elegans* in the absence of external stimuli. *PLoS One*, 8(11):e78535.

Pierce-Shimomura, J. T., Morse, T. M., and Lockery, S. R. (1999). The fundamental role of pirouettes in caenorhabditis elegans chemotaxis. *Journal of Neuroscience*, 19(21):9557–9569.

Richmond, P., Chisholm, R., Heywood, P., Leach, M., and Kabiri Chimeh, M. (2024). Flame gpu.

Sugi, T., Ito, H., Nishimura, M., and Nagai, K. H. (2019). *C. elegans* collectively forms dynamical networks. *Nature Communications*, 10(1):683.

Szigeti, B., Gleeson, P., Vella, M., Khayrulin, S., Palyanov, A., Hokanson, J., Currie, M., Cantarelli, M., Idili, G., and Larson, S. (2014). Openworm: an open-science approach to modeling caenorhabditis elegans. *Frontiers in computational neuroscience*, 8:137.

The C. elegans Sequencing Consortium* (1998). Genome sequence of the nematode *c. elegans*: a platform for investigating biology. *Science*, 282(5396):2012–2018.

Turing, A. M. (1990). The chemical basis of morphogenesis. *Bulletin of mathematical biology*, 52:153–197.

Wan, X., Zhou, Y., Chan, C. M., Yang, H., Yeung, C., and Chow, K. L. (2019). Srd-1 in awa neurons is the receptor for female volatile sex pheromones in *c. elegans* males. *EMBO reports*, 20(3):e46288.

Wang, Z. (2010). On chemotaxis models with cell population interactions. *Mathematical Modelling of Natural Phenomena*, 5:173–190.

White, J. G., Southgate, E., Thomson, J. N., Brenner, S., et al. (1986). The structure of the nervous system of the nematode caenorhabditis elegans. *Philos Trans R Soc Lond B Biol Sci*, 314(1165):1–340.